Evolution of Carbides in GCr15 Bearing Steel during the Quenching Process

Yujun LI *, Jinzhao GUAN, Ming LIN

School of Materials Science and Engineering, Jiujiang University, Jiujiang 332005, Jiangxi, China

http://doi.org/10.5755/j02.ms.36910

Received 8 April 2024; accepted 9 August 2024

The evolution of carbides and the hardness of GCr15 bearing steel specimens during the quenching process were investigated using scanning electron microscopy (SEM) and hardness testing. The volume fraction and size of undissolved carbides under different quenching parameters were analyzed. The results indicated that as the austenitizing time increased from 0 to 25 minutes, the volume fraction of undissolved carbides decreased from 10.77 to 5.72 %, while the mean diameter of undissolved carbides first decreased from 0.264 to 0.214 μm, and then increased to 0.227 μm; as the austenitizing temperature increased from 810 to 930 ℃, the volume fraction decreased from 9.25 % to 0.53 %, while the mean diameter first decreased from 0.238 to 0.222 μm, and then increased to 0.248 μm; as the heating rate increased from 2 to 8 ℃/min, the volume fraction increased from 5.10 to 6.76 %, while the mean diameter decreased from 0.234 to 0.217 μm. It is found that the energy absorbed during austenitization plays a crucial role in the volume fraction and mean diameter of undissolved carbides. That is, before the heat treatment reaches equilibrium or the carbides are fully dissolved, as the energy absorbed during the heat treatment process increases, the volume fraction of undissolved carbides decreases, while the mean diameter of undissolved carbides tends to increase. It is demonstrated that the hardness of the GCr15 bearing steel specimens is closely related to the volume fraction and mean diameter of undissolved carbides. That is, before the coarsening of carbides, the hardness of GCr15 steel specimens gradually increases as the volume fraction of carbides decreases.

Keywords: GCr15 bearing steel, undissolved carbides, quenching, the volume fraction and mean diameter, hardness.

1. INTRODUCTION

GCr15 bearing steel is a common high carbon chromium rolling bearing steel, which is mainly used to manufacture different rollers, shaft sleeves, bearing balls on transmission shafts, and so on [1]. When GCr15 bearing steel is used to manufacture bearing parts, the working environment is harsh, and it can experience contact stresses of up to 3000 MPa [2]. Therefore, the bearing steel generally needs to have extremely high hardness (>653 HV ≈ 58 HRC), good wear resistance, strong tenacity, and high fatigue strength [3 – 7]. The steel grade and service environment determine that the main heat treatment processes for GCr15 bearing steel are spheroidization annealing, quenching, and low temperature tempering. The microstructure of spheroidization annealing is mostly spherical or granular pearlite, to improve machinability. After spheroidization annealing, GCr15 bearing steel will then be subjected to quenching and low temperature tempering treatment in order to enhance hardness, wear resistance, and to possess a certain degree of toughness. In general, for hypereutectoid alloy steels like GCr15 steel, the quenching heating temperature is AC1 + 30 ~ 50 ℃, and the quenching medium is oil to avoid cracking after quenching. The tempering temperature is 150 – 250 ℃, which can reduce the internal stress and brittleness of the steel and maintain its high hardness and wear resistance after quenching. The microstructure of GCr15 bearing steel after quenching and tempering treatment is mainly composed of tempered martensite, dispersed and fine granular carbide, as well as a small amount of retained austenite.

In the above-mentioned three heat treatment processes of GCr15 bearing steel, the quenching process plays a connecting role, whose microstructure parameters have a decisive impact on the final service life of a bearing. On the one hand, accompanied by the transformation from ferrite to austenite, spherical or granular carbides in the spheroidization annealing microstructure of GCr15 bearing steel largely dissolve into austenite or fragment during the austenitizing process before quenching, which greatly enhances lattice distortion after quenching [8], resulting in a sharp increase in solution strengthening. Meanwhile, the undissolved spherical or granular carbides become fine and dispersed [9]. Thus, the second phase dispersion strengthening is enhanced. The combined effect of solution strengthening and second phase dispersion strengthening makes the strength, hardness, and wear resistance of spheroidization annealed GCr15 bearing steel sharply increase after quenching. On the other hand, although the hardness of GCr15 bearing steel after low temperature tempering decreases and its toughness increases, compared with the hardness after quenching, the hardness after low temperature tempering decreases slightly. Alternatively, the hardness after low temperature tempering is close to that after quenching [4]. Accordingly, the strength, hardness, and wear resistance of GCr15 bearing steel are indirectly determined by the quenching process.

During the austenitizing process before quenching, the carbide gradually dissolves into austenite, and austenite

* Corresponding author; Y. Li
E-mail: *netdream@jju.edu.cn*

grain continues to grow. To some extent, the microstructure parameters of quenching are depended on the austenitizing process [11]. It is generally agreed that for high carbon steels such as bearing steel, the mechanical properties such as strength and hardness are closely related to the volume fraction (or area fraction) and size of undissolved carbides, as well as the size and amount of prior austenite grain [10 – 12], among which the volume fraction and size of undissolved carbides directly affect the evolution and properties of the microstructure [13 – 18]. Generally, the size of undissolved carbides should be controlled starting from the spheroidization annealing process. He et al. [19] reported that during the spheroidization annealing process of Cr-Mo-Si-V alloy steel, the microhardness of the sample decreased first quickly and then slowly with the increase of the average diameter of secondary carbides. Li et al. [8] proposed a novel online subcritical spheroidization annealing technology that can be used to refine the size of undissolved carbides after quenching and tempering, and reduce the volume fraction of undissolved carbides, thereby improving the mechanical properties of bearing steel. For quenched microstructure, it is generally desirable that the volume fraction of undissolved carbides is controlled within 3 % – 6 % [20 – 22], which is not only conducive to inhibiting the growth of prior austenite grain by pinning effect, but also serves as a hard phase to prevent wear damage during bearing operation [2]. The volume fraction of undissolved carbides, whether too large or too small, is detrimental to the mechanical properties of bearing steel. For example, it is pointed out in the literature that if the volume fraction was too large, the corresponding strength and hardness would be too low to endure the working conditions of the bearing [12]. On the contrary, Park et al. [23] believed that a low volume fraction of undissolved carbides after quenching and low temperature tempering could indirectly lead to fatigue fracture of high carbon steel.

The changes in the size and volume fraction of undissolved carbides from spheroidizing annealing to quenching are the largest, while the changes from quenching to tempering are very small [1]. However, there was little research on how quenching parameters affect the size and volume fraction of undissolved carbides. In this work, the microstructure evolution behavior in GCr15 bearing steel during the quenching process was analyzed by calculating the size and volume fraction of undissolved carbides. The hardness after quenching was also measured. The relationship between the hardness of GCr15 bearing steel and the volume fraction and size of undissolved carbides are also discussed.

2. EXPERIMENTAL METHODS

The experimental material is GCr15 bearing steel subjected to spheroidization annealing with a size of ∅ 15 × 16 mm. The main chemical component is examined by the spectral analyzer (NSC SparkCCD 7000) and given in Table 1. Based on the chemical composition of the steel grade, the values of the equilibrium temperatures A_1 and A_{cm} at the critical phase transition point were calculated using Jmatpro 6.0 software, as shown in Fig. 1. It is seen from Fig. 1 that the A_1 and A_{cm} temperatures of GCr15 steel are 738 and 890 °C, respectively. According to the principle of heat treatment, the reasonable heating temperature for quenching GCr15 steel should be A_{c1} + (30 – 50 °C), where A_{c1} is the austenitizing temperature at which the ferrite to austenite starts to transform, which is strongly affected by the heating rate [22]. Generally, A_{c1} is higher than the A_1 equilibrium temperature and has a higher value in the higher heating rate. In this experiment, the austenitizing temperature (A_{c1}) was selected based on the A_1 temperature.

Table 1. Main chemical composition of GCr15 bearing steel, wt.%

C	Si	Mn	Cr	P	S
1.0	0.25	0.35	1.50	0.020	0.020

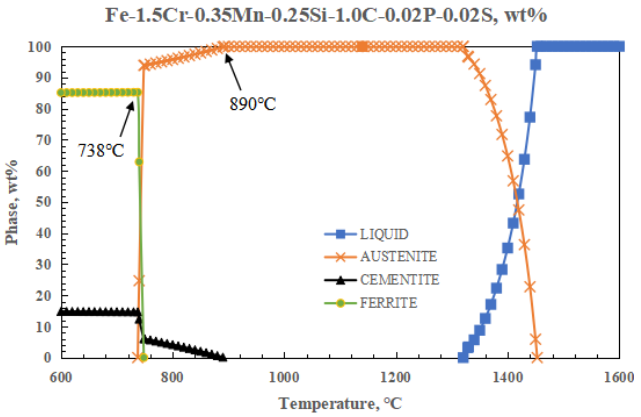

Fig. 1. Temperature chart of A_1 and A_{cm} calculated by Jmatpro software

All these specimens were put into a box type resistance furnace (KSL-1000X) for austenitizing and then subjected to quenching. The progress of each quenching process is described as follows. The specimen was heated at a certain heating rate to the austenitizing temperature, held for some time, and then quickly taken out for oil quenching to room temperature. The detailed quenching parameters are present in Table 2.

Table 2. Quenching parameters of the GCr15 bearing steel

Specimen	Heating rate, °C/min	Austenitizing temperature, °C	Austenitizing time, min
V6T840H0	6	840	0
V6T840H5	6	840	5
V6T840H10	6	840	10
V6T840H15	6	840	15
V6T840H20	6	840	20
V6T840H25	6	840	25
V6T810H20	6	810	20
V6T870H20	6	870	20
V6T900H20	6	900	20
V6T930H20	6	930	20
V2T840H20	2	840	20
V4T840H20	4	840	20
V8T840H20	8	840	20

For microstructural investigation, all the specimens were mechanically processed and polished using a standard metallographic procedure, and then etched with a 4% nitric acid alcohol solution. Microstructure was examined by scanning electron microscope (SEM; ESCAN VEGA II LSU). The hardness was measured by the Rockwell hardness tester with a load of 150 kgf and a holding time of 10 s. The hardness of the specimen **was** demonstrated by the

average of 5 readings. According to the micrographs obtained by SEM, the mean diameter and volume fraction of undissolved carbides were measured using Image-pro Plus 6.0 software. The calculation method for the mean diameter and volume fraction of undissolved carbides can be found in references [8, 25 – 29].

3. RESULTS AND DISCUSSION

3.1. Microstructure after spheroidization annealing

The GCr15 bearing steel specimen used in the experiment was subjected to a spheroidization annealing process, to reduce hardness and facilitating processing. Its microstructure is mainly composed of spherical or granular pearlite (i.e., spherical or granular carbides distributed on the ferrite matrix), as shown in Fig. 2 a. As shown in the figure, the size of carbides after spheroidization varies, and are dispersed and uniformly distributed on the ferrite matrix. In addition, individual thick and big undissolved carbides with a size of about 2.0 μm can be seen in the figure, which are generally believed to be inherited from proeutectoid network carbides [30]. The mean diameter of the carbides was measured, which was 0.24 μm. Fig. 2 b further shows the distribution of carbide size, which is similar to the study by Li et al. [8]. The figure shows that 57.24 % of carbides have a particle size less than 0.2 μm, among which 23.24 % are less than 0.1 μm. But there are still 3.16 % of carbides with a particle size greater than 1.0 μm, among which 0.2 % have a particle size of around 2.0 μm, which is caused by the spheroidizing annealing process [8, 26]. The hardness of the specimen after spheroidization annealing was 21 HRC using the HRSS-150 Rockwell hardness tester, which is suitable for cutting processing and provides microstructural preparation for subsequent quenching.

3.2. Effect of austenitizing time on microstructure evolution

Fig. 3 shows the microstructure evolution in the specimens (V6T840H0, V6T840H5, V6T840H10, V6T840H15, V6T840H20, and V6T840H25) under different austenitizing times.

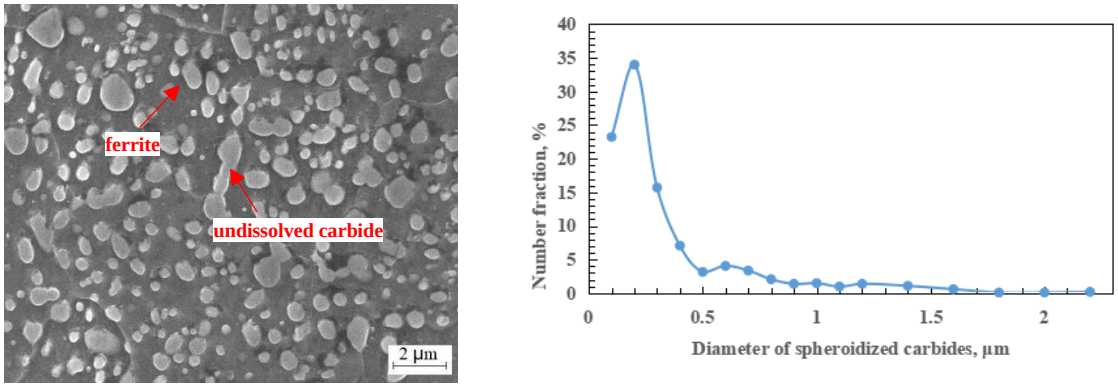

a b

Fig. 2. SEM images showing microstructure and carbide size distribution of the tested steel: a – SEM images; b – carbides size

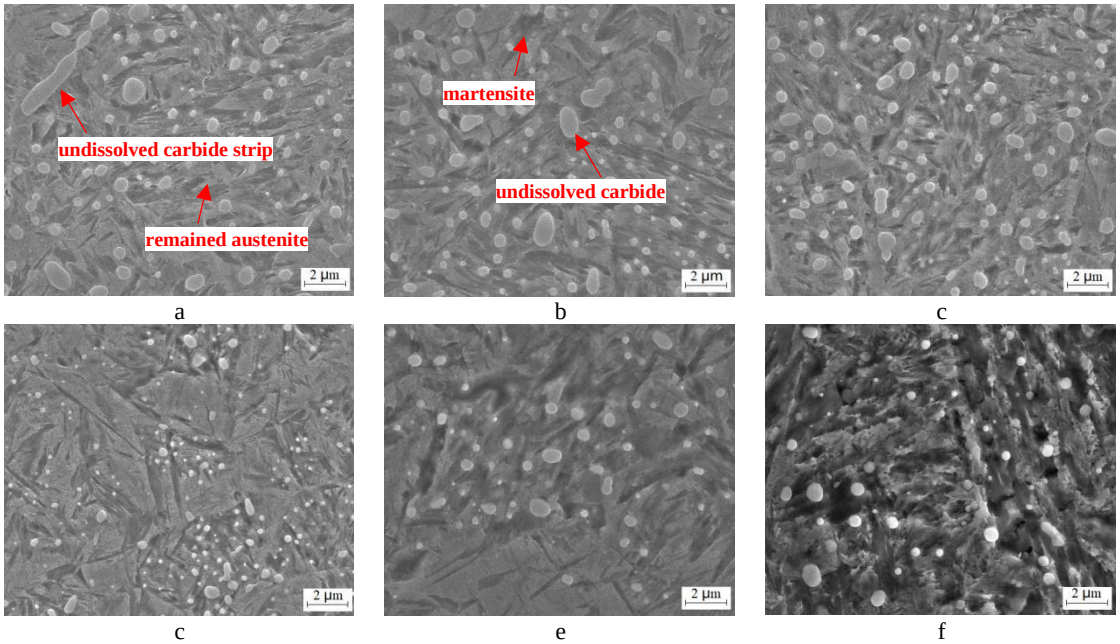

a b c

c e f

Fig. 3. SEM images showing microstructure of specimens with different austenitizing holding times: a – V6T840H0; b – V6T840H5; c – V6T840H10; d – V6T840H15; e – V6T840H20; f – V6T840H25

It can be seen from the figure that the microstructure of the specimen is composed of martensite matrix, carbide distributed thereon and remained austenite. Under different austenitizing times, the morphology of martensite matrix and carbide is quite different. The undissolved carbide strip can still be seen in the specimen without holding time (V6T840H0) due to the heredity from proeutectoid network carbide [30]. As the holding time prolongs, the particle size of carbides gradually decreases and then increases, with the specimen (V6T840H15) holding for 15 minutes having the smallest particle size. It can also be seen from the figure that the martensite is thicker after the longer austenitizing time. As the austenitizing time increases, the austenite grain gradually grows, and the martensite transformed after quenching also becomes coarser accordingly. The volume fraction and mean diameter of undissolved carbides were measured, as shown in Fig. 4. In Fig. 4 a, the "- ∞" represents the volume fraction of carbides in the initial spheroidized microstructure, which is approximately 19.38 % in this work. This value is calculated as 18.31 % using Jampro 6.0 software, while it is approximately 14 – 24 % in other literature [1, 8, 24, 26]. The reason for some errors between the value measured in this work and previous research may be mainly due to differences in calculation method, measurement method, etching time, and microstructure homogeneity [8]. The "∞" represents the volume fraction of equilibrium carbides calculated by Jampro 6.0 software at this austenitizing temperature, which is 3.29 %. From Fig. 4 a, it can be seen that as the austenitizing time increases from 0 to 25 minutes, the volume fraction of undissolved carbides decreases from 10.77 % to 5.72 %. Due to the A_1 temperature (738 ℃) of the specimen being much lower than the set austenitizing temperature, when heated to around A_1 temperature, the carbides in the spherical pearlite begin to fragment or dissolve. When the temperature rises to this austenitizing temperature, the volume fraction of dissolved carbides reaches 8.61 % (= 19.38 % -10.77 %). When the austenitizing time reaches 10 minutes, the undissolved carbides change slowly with temperature, indicating that the dissolution of carbides has begun to approach equilibrium. However, when the austenitizing time is 25 minutes, the volume fraction (5.72 %) of undissolved carbides is still higher than the equilibrium volume fraction (3.29 %), which means that there is still a certain austenitizing time to reach equilibrium.

Accompanied by the dissolution of carbides, the mean diameter of undissolved carbides also changes, as shown in Fig. 4 b. The "-∞'' in the figure represents the mean diameter of carbides in the initial spheroidized microstructure, which is 0.352 μm in this work. When the austenitizing time increases from 0 to 5 minutes, the mean diameter of undissolved carbides decreases from 0.264 to 0.230 μm. The mean diameter deceleration is 6.8×10^{-3} μm/min, which is a significant decrease. From 5 to 15 minutes, the mean diameter of undissolved carbides decreases from 0.230 to 0.214 μm. The mean diameter deceleration is 1.6×10^{-3} μm/min, which is a slow descent. From 15 to 25 minutes, the mean diameter of undissolved carbides even increases from 0.214 to 0.227 μm, which indicates that the undissolved carbide begins to coarsen at this time. Consequently, at the early stage of austenitization, a large amount of carbides dissolve, resulting in a decrease in the mean diameter of undissolved carbides. However, as the austenitizing time prolongs, the carbon content in austenite gradually approaches an equilibrium state, leading to a gradual decrease in the driving force of carbide dissolution. Therefore, the dissolution rate of carbides gradually decreases with the prolongation of austenitizing time. Before approaching equilibrium, undissolved carbide particles start to coarsen at the expense of small-sized undissolved carbide particles due to the reduction of interfacial energy with austenite [31], which is similar to the Ostwald ripening law [33] (i.e., larger particles coarsen and smaller particles dissolve).

3.3. Effect of austenitizing temperature on microstructure evolution

Identical spheroidized microstructure was subjected to quenching treatment under different austenitizing temperatures. Fig. 5 shows the quenched microstructure of specimens under different austenitizing temperatures with an austenitizing time of 20 minute. The microstructure with an austenitizing temperature of 840 ℃ is shown in Fig. 3 e. Under different austenite temperatures, the microstructure is still composed of martensite matrix, carbides distributed thereon and remained austenite. Obviously, compared with the austenitizing time, the austenitizing temperature has a greater impact on the microstructure of GCr15 bearing steel. For the same steel grade, compared with extending the austenitizing time, increasing the austenitizing temperature before reaching the A_{ccm} temperature clearly increases the carbon dissolving ability of austenite, therefore the driving force for carbide dissolution is greater in higher temperatures.

With the increase of austenitizing temperature, the solubility and diffusivity of carbon and chromium in austenite both increase, which are beneficial to the carbides' dissolution. As a result, a significant decrease in the number of undissolved carbides is observed on the electron microscope image as the austenitizing temperature increases. At the austenitizing temperature of 900 ℃, although the temperature has exceeded the A_{cm} temperature of the specimen, due to the short holding time, the dissolution of carbides has not reached the equilibrium state at this temperature, so a small number of undissolved carbides can still be seen. At the austenitizing temperature of 930 ℃, a very small number of undissolved carbides can be observed, indicating that the dissolution of carbides has not yet reached equilibrium in this state.

Fig. 6 further shows the volume fraction and mean diameter of undissolved carbides under different austenitizing temperatures. Compared with the austenitizing time, as the austenitizing temperature increases, the volume fraction of undissolved carbides decreases more significantly (compared to Fig. 4 a and Fig. 6 a), indicating that the austenitizing temperature has a more significant effect on the dissolution of carbides. Comparing Fig. 4 b and Fig. 6 b, it can be seen that when the temperature exceeds 870 ℃, the austenitizing temperature has a more significant effect on the coarsening of undissolved carbides than the austenitizing time.

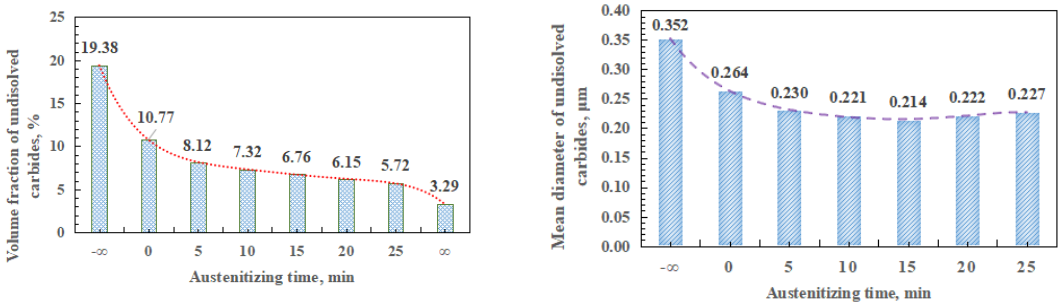

a b

Fig. 4. Volume fraction and mean diameter of undissolved carbide with austenitizing holding time: a – volume fraction; b – mean diameter

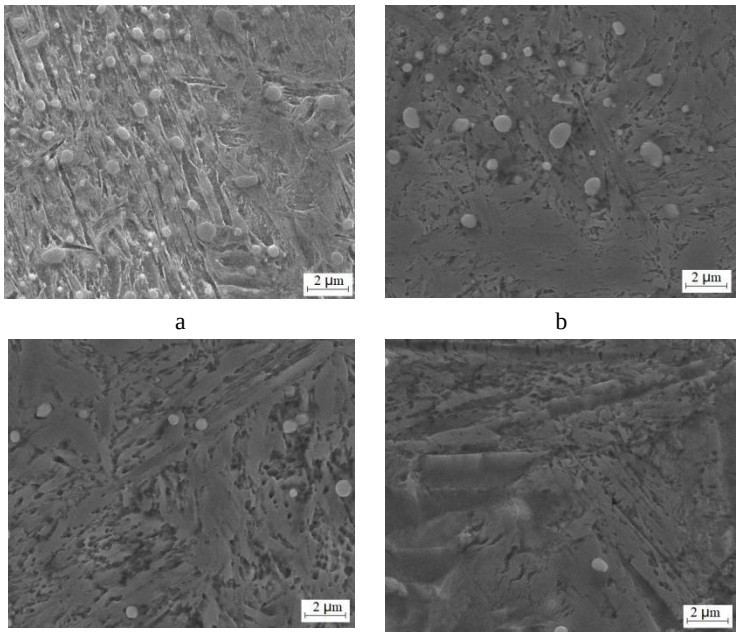

a b

c d

Fig. 5. SEM images showing the microstructure of specimens with different austenitizing temperatures: a – V6T810H20; b – V6T870H20; c – V6T900H20; d – V6T930H20

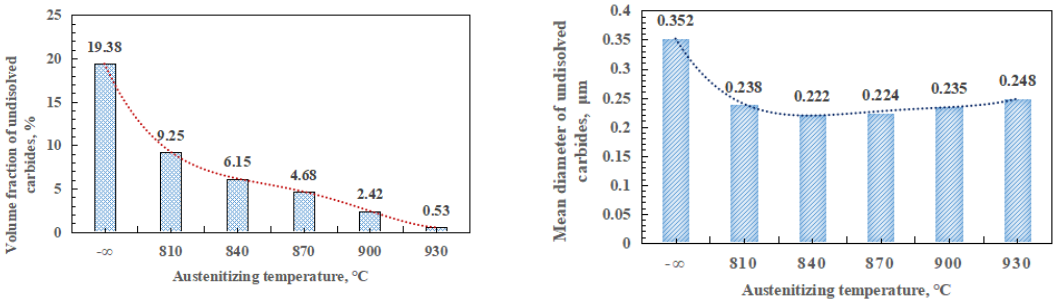

a b

Fig. 6. Volume fraction and mean diameter of undissolved carbide with austenitizing temperature: a – volume fraction; b – mean diameter

3.4. Effect of heating rate on microstructure evolution

The effect of the heating rate on the quenching microstructure of GCr15 steel specimens is shown in Fig. 7. The microstructure with a heating rate of 6 °C/min is shown in Fig. 3 e. Similar to the aforementioned microstructure, the spheroidized undissolved carbide and retained austenite can still be observed on the martensite matrix. From these figures, it can be seen that as the heating rate increases, the volume fraction of undissolved carbides increases, which is mainly attributed to the faster heating rate directly pushing up the temperature at which ferrite transforms into austenite (i.e. A_{c1} temperature). Fig. 8 further shows the volume fraction and mean diameter of undissolved carbides under different heating rates. As the heating rate increases, the volume fraction of undissolved carbides almost linearly increases, while the mean diameter of undissolved carbides decreases slightly. It can be seen that a decrease in heating rate still leads to coarsening of undissolved carbides.

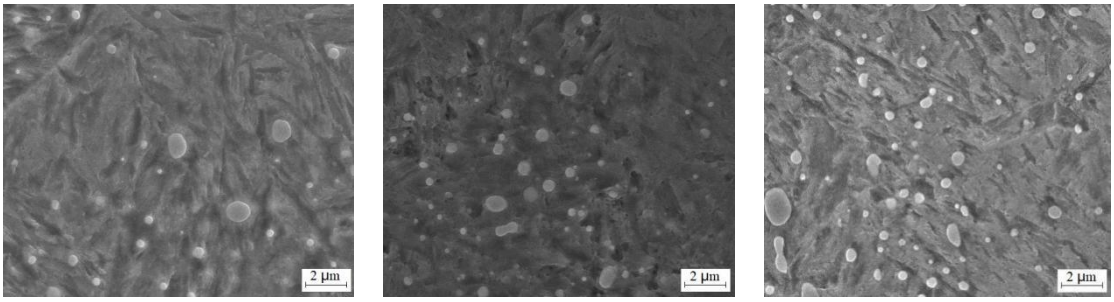

a b c

Fig. 7. SEM images showing microstructure of specimens with different heating rates: a – V2T840H20; b – V4T840H20; c – V8T840H20

Fig. 9 shows a schematic diagram of the heat treatment process. If the shadow area enclosed by the heat treatment curve in the diagram is defined as the energy *Q* absorbed by the specimen during the heat treatment process, that is,

$$Q = \int Tdt \,, \tag{1}$$

where *T* is the heat treatment temperature; *t* is the heat treatment time.

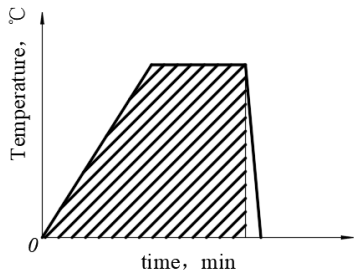

Fig. 9. Schematic diagram of heat treatment process

Based on the influence of quenching parameters on the evolution of quenched microstructure, a general pattern of the influence of quenching parameters on the evolution of undissolved carbides can be summarized. That is, before the heat treatment reaches equilibrium or the carbides are fully dissolved, as the energy absorbed Q during the heat treatment process increases, the volume fraction of undissolved carbides decreases, while the mean diameter of undissolved carbides tends to increase.

As a consequence, the rationality of the selected quenching parameters can be determined based on the energy absorbed by the specimen during the quenching process, which provides a new idea for the rationality of selecting quenching parameters. The absorbed energy is too high, and although the volume fraction of undissolved carbides decreases, the mean diameter increases due to coarsening, resulting in mechanical properties such as hardness that may not be suitable. On the contrary, if the absorbed energy is too low, the volume fraction of undissolved carbides is too high, and then the required mechanical properties cannot be also obtained. However, it should be emphasized that there is still no quantification of the extent to which the absorbed energy is appropriate, so further research is needed.

3.5. Quenching hardness

Due to different microstructure parameters, the hardness of the specimen also varies. The relationship between different quenching parameters and hardness is present in Fig. 10. From the figure, it can be seen that the hardness of GCr15 bearing steel specimens varies between 60 and 66 HRC with different quenching parameters. Among them, when the austenitizing time increases from 0 to 25 minutes, the hardness of the specimen first increases from 60.0 HRC to 65.5 HRC, reaches its maximum at 15 minutes of austenitizing time, and then slightly decreases to 64.5 HRC, as shown in Fig. 10 a. When the austenitizing temperature increases from 810 to 930 ℃, the hardness of the specimen first increases from 63.1 HRC to 65.8 HRC, reaches its maximum at the austenitizing temperature of 870 ℃, and then slowly decreases to 64.9 HRC. When the heating rate increases from 2 to 8 ℃/min, the hardness of the specimen decreases from 65.6 HRC to 64.3 HRC.

The following is an explanation of the relationship between the hardness of GCr15 bearing steel and the austenitizing time based on the evolution of quenched microstructure, especially the volume fraction and size of undissolved carbides. For GCr15 bearing steel, hardness is related to the volume fraction and size of undissolved carbides, as well as the size and amount of prior austenite grain [10 – 12]. Generally, a smaller volume of undissolved carbide, as well as finer undissolved carbide particles and prior austenite grain size, will increase the hardness of the quenched microstructure [8]. As shown in Fig. 4, when the specimen was quenched at the austenitizing temperature and without holding time, 8.61 % volume fraction of carbide dissolved into austenite, and the mean diameter of the undissolved carbide was 0.264 μm. Compared with the spheroidized annealing microstructure, the volume fraction and mean diameter of undissolved carbides decreased by 44.43 % and 32.39 %, respectively. That is, the dissolved carbide in austenite and subsequently quenched martensite increased by 44.43 %, and the decrease of 32.39 % in mean diameter resulted in finer and more dispersed carbides. Under the double strengthening of solution strengthening and second phase dispersion strengthening, the hardness of the quenched microstructure of the specimen reached 60.0 HRC. Compared with the hardness (21 HRC) of spheroidization annealing microstructure, the hardness significantly increases by 185.71 % [23]. When the austenitizing time is 5 minutes, the volume fraction and mean diameter of undissolved carbides are 8.12 % and 0.230 μm, respectively, which is further decreased by 24.61 % and 12.88 %, respectively, compared with the austenitizing time of 0 min.

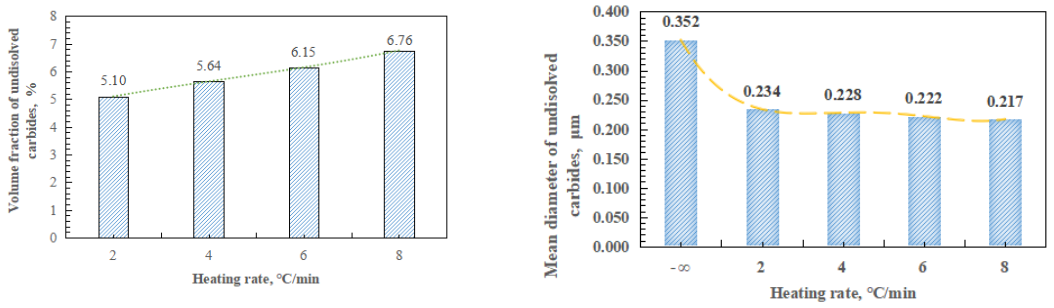

a b

Fig. 8. Volume fraction and mean diameter of undissolved carbide with heating rate: a – volume fraction; b – mean diameter

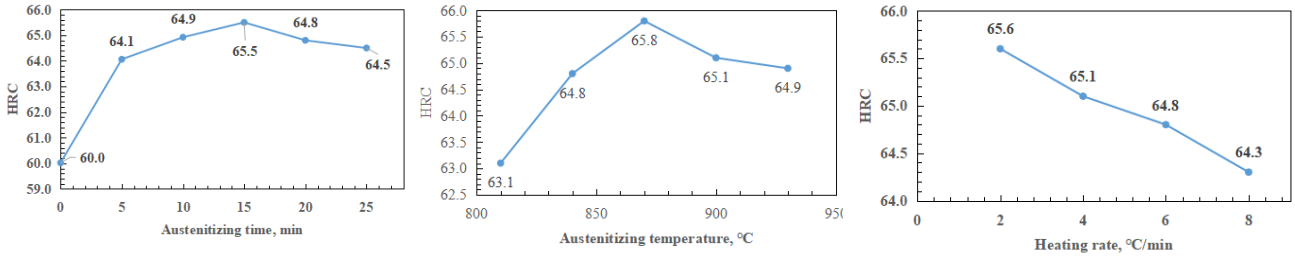

a b c

Fig. 10. The relationship between hardness and quenching parameters of the GCr15 bearing specimens: a – austenitizing time; b – austenitizing temperature; c – heating rate

The solution strengthening and the second phase dispersion strengthening were further strengthened. As a result, the hardness increased to 64.1 HRC, with an increase of 6.83 %. As the austenitizing time further increased to 15 minutes, the volume fraction and mean diameter of undissolved carbides in austenite only decreased by 16.75 % and 6.96 %, respectively. Therefore, the hardness increased slowly, with an increase of only 2.18 %. Subsequently, when the austenitizing time increased from 15 to 25 minutes, the decrease in volume fraction of undissolved carbides was slower, only 15.38%. The mean diameter even increased by 6.07 % due to coarsening. In addition, the size and amount of the prior austenite grain increase with the increase of austenitizing time [32]. Therefore, when the austenitizing time exceeded 15 minutes, the hardness slowly decreased with the increase of austenitizing time. It can be seen that before the coarsening of carbides, the hardness of GCr15 steel specimens gradually increases as the volume fraction of carbides decreases.

Similarly, the variation of hardness with austenitizing temperature and heating rate can also be explained based on the volume fraction and mean diameter of undissolved carbides, as well as the changes in the size and amount of the prior austenite grain, and will not be further elaborated here.

4. CONCLUSIONS

The evolution of microstructure and hardness of GCr15 bearing steel under different quenching parameters were investigated in this work. The main conclusions are summarized as follows:

1. As the austenitizing time increases from 0 to 25 minutes, the volume fraction of undissolved carbides decreased from 10.77 to 5.72 %, while the mean diameter of undissolved carbides first decreased from 0.264 to 0.214 μm, and then increased to 0.227 μm.
2. As the austenitizing temperature increases from 810 to 930 °C, the volume fraction decreases from 9.25 % to 0.53 %, while the mean diameter first decreases from 0.238 to 0.222 μm, and then increases to 0.248 μm.
3. As the heating rate increases from 2 to 8 °C/min, the volume fraction increases from 5.10 to 6.76 %, while the mean diameter decreases from 0.234 to 0.217 μm.
4. Before the heat treatment reaches equilibrium or the carbides are fully dissolved, the more energy absorbed during the austenitization process, the smaller the volume fraction of undissolved carbides, and the mean diameter of undissolved carbides tends to increase.
5. The quenching microstructure of GCr15 steel specimen is composed of martensite matrix, carbide distributed hereon and retained austenite. The hardness is 60 ~ 66 HRC, and is closely related to the volume fraction and mean diameter of undissolved carbide. That is, before the coarsening of carbides, the hardness of GCr15 steel specimens gradually increases as the volume fraction of carbides decreases.

REFERENCES

1. **Ma, C., Luo, H.** Precipitation and Evolution Behavior of Carbide during Heat Treatments of GCr15 Bearing Steel *Journal of Materials Engineering* 45 (6) 2017: pp. 97 – 103 (in Chinese). https://doi.org/10.11868/j.issn.1001-4381.2016.001092
2. **Cui, W., San-Martín, D., Rivera-Díaz-del-Castillo, P.E.J.** Towards Efficient Microstructural Design and Hardness Prediction of Bearing Steels – An Integrated Experimental

and Numerical Study *Materials & Design* 133 2017: pp. 464 – 475. https://doi.org/10.1016/j.matdes.2017.08.013

3. **Li, D., He, W., Zhang, X.** Effects of Traditional Heat Treatment and a Novel Deep Cryogenic Treatment on Microstructure and Mechanical Properties of Low-Carbon High-Alloy Martensitic Bearing Steel *Journal of Iron and Steel Research International* 28 (3) 2021: pp. 370 – 382. https://doi.org/10.1007/s42243-020-00527-5
4. **Bhadeshia, H.** Steels for Bearings *Progress in Materials Science* 57 (2) 2012: pp. 268 – 435. https://doi.org/10.1016/j.pmatsci.2011.06.002
5. **Rivolta, B., Gerosa, R., Sala, C., Tavasci, F., Angelini, L., Bolognani, N., Panzeri, A., Parimbelli, A.** Influence of Prior Microstructure on the Mechanical and Microstructural Properties of C–Mn–B Steel after Spheroidizing Annealing *Ironmaking & Steelmaking* 48 (9) 2021: pp. 1013 – 1021. https://doi.org/10.1080/03019233.2020.1858223
6. **Kose, C.** Dissimilar Laser Beam Welding of AISI 420 Martensitic Stainless Steel to AISI 2205 Duplex Stainless Steel: Effect of Post-Weld Heat Treatment on Microstructure and Mechanical Properties *Journal of Materials Engineering and Performance* 30 (10) 2021: pp. 7417 – 7448. https://doi.org/10.1007/s11665-021-06071-x
7. **Kose, C.** Effect of Heat Input and Post Weld Heat Treatment on the Texture Microstructure and Mechanical Properties of Laser Beam Welded AISI 317L Austenitic Stainless Steel *Materials Science and Engineering A* 855 2022: pp. 143966. https://doi.org/10.1016/j.msea.2022.143966
8. **Li, C., Li, Z., Ren, J., Tu, X., Li, B.** Microstructure and Properties of 1.0C – 1.5Cr Bearing Steel in Processes of Hot Rolling, Spheroidization, Quenching, and Tempering *Steel Research International* 90 (3) 2019: pp. 1800470. https://doi.org/10.1002/srin.201800470
9. **Barrow, A.T.W.P., Rivera-Díaz-del-Castillo, E. J.** Nanoprecipitation in Bearing Steels *Acta Materialia* 59 (19) 2011: pp. 7155 – 7167. https://doi.org/10.1016/j.actamat.2011.08.007
10. **Cao, Z., Shi, Z., Yu, F., Sugimoto, K., Cao, W., Weng, Y.** Effects of Double Quenching on Fatigue Properties of High Carbon Bearing Steel with Extra-High Purity *International Journal of Fatigue* 128 2019: pp. 105176. https://doi.org/10.1016/j.ijfatigue.2019.06.036
11. **Li, Z., Li, C., Ren, J., Li, B., Zhang, J., Ma, Y.** Effect of Cold Deformation on the Microstructure and Impact Toughness during the Austenitizing Process of 1.0 C – 1.5 Cr Bearing Steel *Materials Science and Engineering A* 674 2016: pp. 262 – 269. https://doi.org/10.1016/j.msea.2016.07.105
12. **Li, Z., Li, C., Ren, J., Li, B., Suh, D.** Design of Online Spheroidization Process for 1.0C – 1.5Cr Bearing Steel and Microstructure Analysis *Metallurgical and Materials Transactions A* 49 2018: pp. 1782-1794. https://doi.org/10.1007/s11661-018-4511-9
13. **Prat, O., García, J., Rojas, D., Sanhueza, J.P., Camurri, C.** Study of Nucleation, Growth and Coarsening of Precipitates in a Novel 9 % Cr Heat Resistant Steel: Experimental and Modeling *Materials Chemistry and Physics* 143 (2) 2014: pp. 754 – 764. https://doi.org/10.1016/j.matchemphys.2013.10.010
14. **Li, Z., Li, C., Zhang, J., Li, B., Pang, X.** Microstructure of Hot Rolled 1.0 C – 1.5 Cr Bearing Steel and Subsequent Spheroidization Annealing *Metallurgical and materials transactions A* 47 2016: pp. 3607 – 3621. https://doi.org/10.1007/s11661-016-3425-7
15. **Li, Z., Li, C., Zhang, J., Qiao, B., Li, Z.** Effects of Annealing on Carbides Size and Distribution and Cold Formability of 1.0 C-1.5 Cr Bearing Steel *Metallurgical and Materials Transactions A* 46 2015: pp. 3220 – 3231. https://doi.org/10.1007/s11661-015-2904-6
16. **Long, X., Zhang, F., Yang, Z., Yang, Z., Lv, B.** Study on Microstructures and Properties of Carbide-Free and Carbide-Bearing Bainitic Steels *Materials Science and Engineering A* 715 2018: pp. 10 – 16. https://doi.org/10.1016/j.msea.2017.12.108
17. **Zhao, L., Vermolen, F., Wauthier, A., Sietsma, J.** Cementite Dissolution at 860 °C in an Fe-Cr-C Steel *Metallurgical and Materials Transactions A* 37 2006: pp. 1841 – 1850. https://doi.org/10.1007/s11661-006-0127-6
18. **Lee, S., Clarke, K.** A Quantitative Investigation of Cementite Dissolution Kinetics for Continuous Heating of Hypereutectoid Steel *Metallurgical and Materials Transactions A* 46 2015: pp. 3917 – 3923. https://doi.org/10.1007/s11661-015-2995-0
19. **He, S., Li, C., Ren, J., Gao, C., Zhang, Y.** Evolution of Carbides in Cr–Mo–Si–V Alloy Steel during the Spheroidization Annealing Process *Steel Research International* 91 (1) 2020: pp. 1900287. https://doi.org/10.1002/srin.201900287
20. **Pandit, A.S., Bhadeshia, H.** Divorced Pearlite in Steels *Proceedings of the Royal Society A*: *Mathematical, Physical and Engineering Sciences* 468 2012: pp. 2767 – 2778. https://doi.org/10.1098/rspa.2012.0115
21. **Barrow, A.T.W.J., Kang, H., Rivera-Díaz-del-Castillo, P.E.J.** The $\epsilon \rightarrow \eta \rightarrow \theta$ Transition in 100Cr6 and Its Effect on Mechanical Properties *Acta Materialia* 60 (6 – 7) 2012: pp. 2805 – 2815. https://doi.org/10.1016/j.actamat.2012.01.046
22. **Zhao, J., Zhao, T., Hou, C., Zhang, F., Wang, T.** Improving Impact Toughness of High-C–Cr Bearing Steel by Si–Mo Alloying and Low-Temperature Austempering *Materials & Design* 86 2015: pp. 215 – 220. https://doi.org/10.1016/j.matdes.2015.07.055
23. **Park, K., Cho, S., Lee, K., Kim, G., Lee, C.** Effect of Volume Fraction of Undissolved Cementite on the High Cycle Fatigue Properties of High Carbon Steels *International journal of fatigue* 29 2007: pp. 1863 – 1867. https://doi.org/10.1016/j.ijfatigue.2007.01.001
24. **Epp, J., Surm, H., Kessler, O., Hirsch, T.** In-situ X-ray Investigations and Computer Simulation during Continuous Heating of a Ball Bearing Steel *Metallurgical and Materials Transactions A* 38 2007: pp. 2371 – 2378. https://doi.org/10.1007/s11661-007-9314-3
25. **Lv, Z., Sun, S., Wang, Z., Qv, M., Fu., W.** Effect of Alloying Elements Addition on Coarsening Behavior of Pearlitic Cementite Particles after Severe Cold Rolling and Annealing *Materials Science and Engineering A* 489 2008: pp. 107 – 112. https://doi.org/10.1016/j.msea.2007.12.005
26. **Song, W., Choi, P., Inden, G., Prahl, U., Raabe, D., Bleck, W.** On the Spheroidized Carbide Dissolution and Elemental Partitioning in High Carbon Bearing Steel 100Cr6 *Metallurgical and Materials Transactions A* 45 2014: pp. 595 – 606. https://doi.org/10.1007/s11661-013-2048-5

27. **Kose, C., Topal, C.** Dissimilar Laser Beam Welding of AISI 2507 Super Duplex Stainless to AISI 317L Austenitic Stainless Steel Materials *Science and Engineering A* 862 2023: pp. 144476. https://doi.org/10.1016/j.msea.2022.144476
28. **Kose, C., Topal, C.** Effect of Heat Input and Post-Weld Heat Treatment on Surface, Texture, Microstructure, and Mechanical Properties of Dissimilar Laser Beam Welded AISI 2507 Super Duplex to AISI 904L Super Austenitic Stainless Steels *Journal of Manufacturing Processes* 73 2022: pp. 861 – 894. https://doi.org/10.1016/j.jmapro.2021.11.040
29. **Kose, C., Topal, C.** Texture, Microstructure and Mechanical Properties of Laser Beam Welded AISI 2507 Super Duplex Stainless Steel *Materials Chemistry and Physics* 289 2022: pp. 126490. https://doi.org/10.1016/j.matchemphys.2022.126490
30. **Han, H., Zhao, X., Zhao, X., Wan, C., Wang, W.** Effect of Proeutectoid Carbide on Heredity in Microstructure-Mechanical Properties and Fatigue Life of GCr15 Bearing Steel *Metallurgical Research & Technology* 114 (2) 2017: pp. 208. https://doi.org/10.1051/metal/2017009
31. **Hecht, M.D., Picard, Y.N., Webler, B. A.** Coarsening of Inter-and Intra-Granular Proeutectoid Cementite in an Initially Pearlitic 2c-4cr Ultrahigh Carbon Steel *Metallurgical and Materials Transactions A* 48 2017: pp. 2320 – 2335. https://doi.org/10.1007/s11661-017-4012-2
32. **Maropoulos, S., Karagiannis, S., Ridley, N.** The Effect of Austenitising Temperature on Prior Austenite Grain Size in a Low-Alloy Steel *Materials Science and Engineering A* 483 2008: pp. 735 – 739. https://doi.org/10.1016/j.msea.2006.11.172
33. **Hwang, K., Lee, S., Lee, H.** Effects of Alloying Elements on Microstructure and Fracture Properties of Cast High Speed Steel Rolls: Part II. Fracture Behavior *Materials Science and Engineering A* 254 1998: pp. 296 – 304. https://doi.org/10.1007/s11661-005-0141-0